Talanta 82 (2010) 1845–1852

Contents lists available at ScienceDirect

Talanta

journal homepage: www.elsevier.com/locate/talanta

Facile synthesis of urchin-like gold submicrostructures for nonenzymatic glucose sensing

Fugang Xu[a,b], Kang Cui[a,b], Yujing Sun[a,b], Cunlan Guo[a,b], Zhelin Liu[a,b], Yue Zhang[a,b], Yan Shi[a,b], Zhuang Li[a,*]

[a] State Key Laboratory of Electroanalytical Chemistry, Changchun Institute of Applied Chemistry, Chinese Academy of Science, RenMin Street 5625, Changchun 130022, Jilin, PR China
[b] Graduate School of the Chinese Academy of Sciences, Beijing 100039, PR China

ARTICLE INFO

Article history:
Received 9 May 2010
Received in revised form 29 July 2010
Accepted 31 July 2010
Available online 7 August 2010

Keywords:
Urchin-like gold submicrostructures
Glucose
Nonenzymatic sensor
Three-dimensional nanostructures
Electrocatalysis
Electrochemical detection

ABSTRACT

Urchin-like gold submicrostructures (UGS) were successfully synthesized by a seed-mediated method which is quite facile and does not need any template or surfactant agent. The effect of the added silver seeds on the morphology and size of final products were investigated, and a possible growth mechanism of crystals was proposed. Electrochemical characterization indicated that these UGS have better catalytic activity for the glucose oxidation compared with flower-like gold submicrostructures (FGS), which could be ascribed to its higher surface to volume ratio. An electrochemical nonenzymatic glucose sensor was fabricated simply by casting the UGS and Nafion solution onto glass carbon electrode. This sensor displays a wide linear range from 0.2 to 13.2 mM with a high sensitivity of 16.8 $\mu A\,mM^{-1}\,cm^{-2}$, and a detection limit of 10 μM. The unique properties of this sensor, such as fast response and well stability reveal the potential application of the UGS based materials in nonenzymatic detection of glucose.

1. Introduction

At present time, three-dimensional (3-D) micro- and nanomaterials with complex structures attracted intensive research interests [1–5]. Much effort has been devoted to the synthesis of 3-D complex structures of gold and silver due to their unique properties and wide applications in optical, electronic and catalytic fields [6–11]. Various strategies, such as electrochemical method, template method and direct chemical reduction method have been developed to prepare gold and silver 3-D complex structures [12–14]. The electrochemical synthesis is fast, but the obtained product has large size (usually on the scale of micrometers), which impairs their performance in some areas, such as electrochemisty and surface enhanced Raman scattering (SERS) [15,16]. The template method is thought to be effective in morphological control, but the limited variety of templates and the tedious post-synthetic treatment restrict its application [11,17]. The direct chemical reduction may be the simplest method, which does not need any exotic power or template. However, most of the prepared structures are flower-like structures built with 2-D nanoflakes or dendritic structures with limited branches (less than 10 branches) [18,19], which have relatively low active surface area. Up to now, few papers have reported the facile synthesis of well-shaped, multi-branched, urchin-like micro- and nanostructures, which may have higher surface to volume ratio.

On the other hand, the reliable, accurate and rapid detection of glucose is of great importance in various areas, such as clinical biochemistry and food industry [20]. Most previous studies on this subject were focused on biosensors based on glucose oxidase [21,22]. However, the enzymes used for biosensors are relatively expensive and they are critical about environmental conditions due to their inherent instability [23]. Moreover, active mediators were usually used to facilitate the electron transfer between the electrode and enzyme [24]. But the leakage of small mediator makes the modified electrode unstable and difficult to control [25]. It is therefore necessary to develop a simple, enzyme-free and mediator-less system for highly sensitive detection of glucose. Functional inorganic nanomaterials especially novel metal materials have been used to achieve this aim due to their particular catalytic activity and well stability. For instance, platinum–carbon nanocomposites and porous gold networks have been fabricated for the nonenzymatic detection of glucose [26,27]. However, the morphologies of these materials are different to control and the fabrication processes are relatively complicated.

In this study, we developed a seed-mediated approach to prepare 3-D urchin-like gold submicrostructures (UGS). This present

* Corresponding author. Tel.: +86 431 85262057; fax: +86 431 85262057.
E-mail address: zligroup@yahoo.com.cn (Z. Li).

0039-9140/$ – see front matter © 2010 Elsevier B.V. All rights reserved.
doi:10.1016/j.talanta.2010.07.087

method is fast and it does not need any strong capping agent or template. The effects of added seeds on the morphology and size of final products were investigated in detail. Importantly, electrochemical characterization indicated that the as-prepared UGS with many nanothorns on their surface had higher active surface area than flower-like gold submicrostructures (FGS). Moreover, the UGS modified electrode exhibited a good catalysis for the oxidation of glucose, and a nonenzymatic glucose sensor with fast response, high sensitivity and good long-term stability was successfully fabricated based on the UGS.

2. Experimental

2.1. Materials

Chloroauric acid ($HAuCl_4{\cdot}4H_2O$), hydrochloric acid (HCl, 36%), sodium hydrogen phosphate ($NaH_2PO_4{\cdot}2H_2O$ and $Na_2HPO_4{\cdot}12H_2O$), sodium citrate ($Na_3C_6H_5O_7{\cdot}2H_2O$) and silver nitrate ($AgNO_3$) were purchased from Beijing Chemical Co. (Beijing, China) with analytical grade. Dopa (3,4-dihydroxyphenylalanine) was purchased from Alfa-Aesar. β-D-glucose was purchased from Shanghai Sinopharm Chemical Reagent Co., Ltd. (Shanghai, China). All chemicals were used as received without further purification. Glassware was cleaned in aqua regia and rinsed with deionized water thoroughly. Ultrapure water (18.2 MΩ cm) was used as solvent throughout this work.

2.2. Apparatus

Scanning electron microscopy (SEM) measurements were made on a XL30 ESEM FEG scanning electron microscope at an accelerating voltage of 20 kV equipped with a Phoenix energy dispersive X-ray analyzer (EDAX). Transmission electron microscopy (TEM) characterization was performed on a JEOL JEM-1011 transmission electron microscope operating at 100 kV. The X-ray diffraction (XRD) analysis was carried out on a D/Max 2500 V/PC X-ray diffractometer using Cu (40 kV, 200 mA) radiation. The samples for SEM and XRD characterization were prepared by dropping 20 μL UGS onto indium tin oxide (ITO) glass slides and microscope slides, respectively. The samples for TEM characterization were prepared by dropping 6 μL UGS onto a carbon-coated copper grid and dried at room temperature. UV–vis–NIR absorbance spectra of UGS in aqueous solution were collected on a Perkin-Elmer λ-900 UV–vis–NIR spectrometer. All electrochemical experiments were performed on a CHI 660A electrochemical workstation (CH Instruments, Chenhua Co., Shanghai, China). A conventional three-electrode system was employed with a bare or modified glassy carbon (3.0 mm in diameter) electrode (GCE) as working electrode, a platinum wire as auxiliary electrode and a KCl saturated Ag/AgCl electrode as reference electrode. Magnetic stirring was kept on mildly through out amperometric measurements.

2.3. Synthesis of UGS and other gold submicrostructures

The silver nanoseeds used here (about 40 nm in diameter) were prepared according to the typical method reported by Lee and Meisel [28]. Briefly, 9 mg silver nitrate was added into 50 mL water. After the solution was boiled, 1.2 mL of 1% sodium citrate was added and the mixed solution was boiled for another 40 min. The yellowish green sol was collected and its volume was fixed at 50 mL.

For the preparation of UGS, 1.0 mL Dopa aqueous solution (12 mM) was mixed with 2.9 mL water. Then, 0.1 mL of the as-prepared silver nanoseeds was added. After adding 1 mL $HAuCl_4$ (12 mM) to the solution, the mixture was gently shaken for several seconds to make it homogenous. The color of the mixed solution changed from light yellow to yellowish gray immediately. After 10 min, dark brown suspension containing UGS formed. The product was collected by centrifugation at 5000 rpm for 5 min, then washed by diluted HCl (~1 M) and distilled water. The obtained product $^{0.1}$UGS (note: the superscript indicates the amount of added seed in milliliter unit) was used for further characterization. Other synthesis processes were modified to the typical method (e.g., introducing different amount of silver nanoseeds into the reaction solution). All the reactions were carried out at room temperature (17 ± 3 °C). The volume of all the final reaction solution was kept at 5 mL and the concentration of gold precursor was kept at 2.4 mM.

2.4. Preparation of UGS modified electrode

Glassy carbon electrode (GCE) was polished before each experiment with 1, 0.3 and 0.05 μm alumina slurry, and then successively washed with diluted nitric acid, acetone and distilled water in ultrasonic bath, respectively. The original suspension containing UGS (5 mL) was concentrated to 400 μL, and then 8 μL of the concentrated suspension was dropped onto the pretreated GCE and dried in the air. After that, 4 μL Nafion (0.1%) was cast onto the electrode. Such modified electrode (UGS/GCE) was used for the cyclic voltammetry experiments and amperometric measurements. The modified electrode was stored at 4 °C when not used.

3. Results and discussion

3.1. Characterization of UGS

The morphology of the as-prepared $^{0.1}$UGS was characterized by SEM and TEM. As can be seen in Fig. 1a, large quantities of "spherical" particles with uniform diameter (261 ± 32 nm, inset of Fig. 1a) were obtained. A close-up view shows there are lots of "nanothorns" on the surface of the product (Fig. 1b and c). The product is in high purity since almost no byproduct presented. The highly magnified TEM image further reveals that lots of (more than ten) dagger-like nanorods radiate out from the solid core (Fig. 1d), which endows the product with a well-shaped urchin-like morphology.

The chemical composition of the $^{0.1}$UGS was analyzed by EDAX and XPS (Fig. 2a and b). The EDAX result clearly display the dominant peak of element Au, demonstrating that the $^{0.1}$UGS is mainly composed of metallic Au (Fig. 2a). The element Ag was from the seed and other elements are from the ITO substrate and the derivative of Dopa. XPS experiment was also performed for the surface analysis of $^{0.1}$UGS (Fig. 2b). The significant Au 4f signal at 83.7 and 86.5 eV further confirms the material is metallic Au.

XRD analysis was used to characterize the crystal structure of $^{0.1}$UGS (Fig. 2c). Five sharp peaks are identified to be the (1 1 1), (2 0 0), (2 2 0), (3 1 1) and (2 2 2) diffraction peaks of fcc gold (JCPDS, No. 04-0784), indicating that the $^{0.1}$UGS is made of crystal Au. It should be noted that the intensity ratio of peak (1 1 1) to (2 0 0) is higher than the standard diffraction data (3.1 vs. 1.9), which suggests that the $^{0.1}$UGS has a tendency to grow with the surface dominated by the lowest energy (1 1 1) facets [29]. The $^{0.1}$UGS in aqueous solution was characterized by UV–vis–NIR (Fig. 2d). The surface plasmon resonance peak shifts to the near infrared range compared with spherical gold nanoparticles, which indicates the $^{0.1}$UGS obtained here has relatively large particle size (submicrometers) [30]. However, the diameters of UGSs in this work are much smaller than that of previously reported architecture fabricated by gold nanowire assembly and other flower-like structures [31,32].

3.2. Effect of nanoseeds on the formation of UGS

A control experiment was performed to identify the role of the silver nanoseeds in the formation of UGS. Dopa and $HAuCl_4$

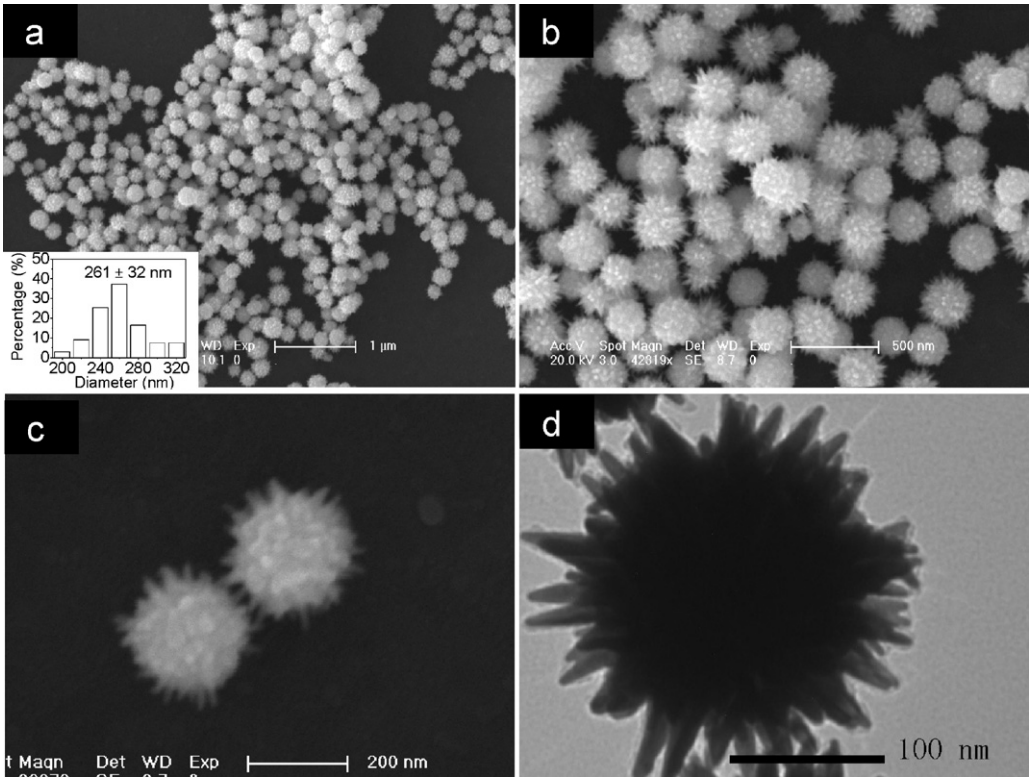

Fig. 1. (a–c) Different magnified SEM images and (d) enlarged TEM image of as-prepared $^{0.1}$UGS. The inset of a shows the size distribution of as-prepared $^{0.1}$UGS.

were reacted at the same condition as that of the typical synthetic process, except that no nanoseeds were added. Fig. 3 shows the typical SEM and TEM images of products obtained in the absence of nanoseeds. It is clear that no urchin-like product but flower-like gold submicrostructures (FGS) composed of nanosheets were formed (Fig. 3a and b). This result clearly declares that the introduced silver nanoseeds are critical to the formation of UGS. As previously reported, the silver nanoseed could act as a nucleation and accumulation center, catalyzing the growth and attachment of primary particles and finally leading to different products [33].

While the presence of silver nanoseeds benefits the formation of UGS, the size of UGS could be tuned by adding different amount of nanoseeds to the reaction solution. Fig. 4 displays the morphology and size distribution of products obtained in the presence of different amount of silver nanoseeds. It is obvious that all the products obtained here exhibit urchin-like morphology (Fig. 4). The

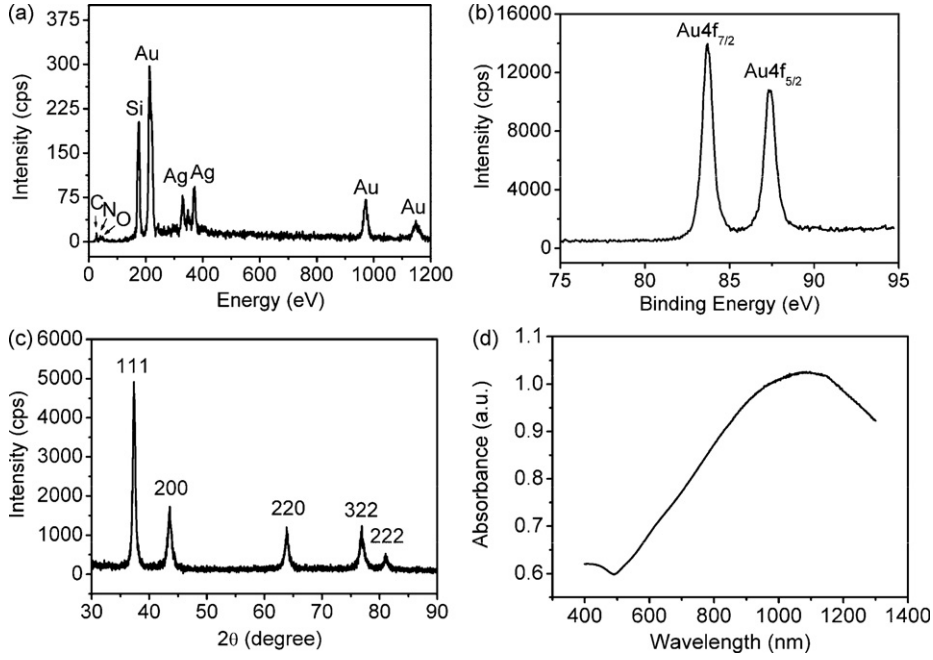

Fig. 2. The (a) EDAX spectrum, (b) XPS spectrum (Au 4f) and (c) XRD pattern of as-prepared $^{0.1}$UGS on substrates and (d) UV–vis–NIR absorption spectrum of $^{0.1}$UGS in aqueous solution.

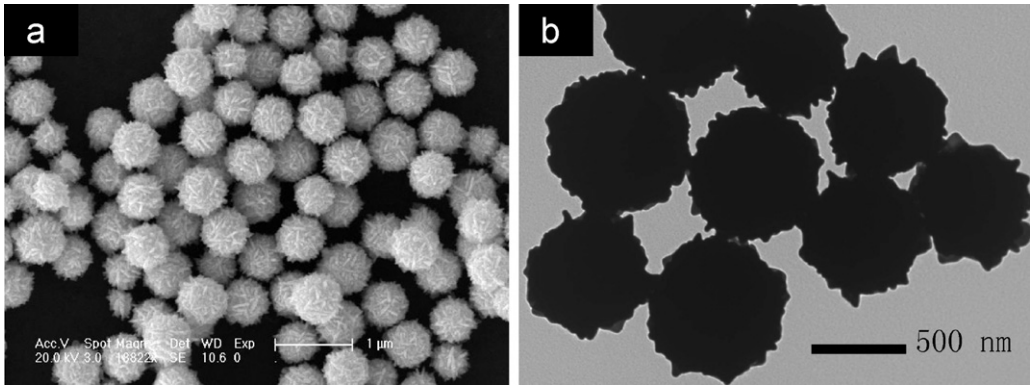

Fig. 3. (a) SEM image and (b) enlarged TEM image of flower-like gold submicrostructures (FGS) obtained in the absence of nanoseed.

statistic results from SEM images clearly show the average product size decreases from 261 ± 32 nm (inset of Fig. 1a) to 205 ± 30 nm (inset of Fig. 4a), and further down to 169 ± 19 nm (inset of Fig. 4c, $^{0.5}$UGS) when the amount of nanoseeds was increased from 0.1 to 0.2 and 0.5 mL, respectively. It is easy to understand this variety of particle size. Since the concentrations of $HAuCl_4$ and Dopa are constant in this seed-mediated approach, it is speculated that the amount of the primary gold crystals reduced by Dopa is almost the same. When more seeds are added, less primary crystals (i.e., the gold source of UGS growth) are available to an individual core (i.e., the nanoseed), which decreases the diameter of resultant UGS.

3.3. Growth mechanism of UGS

The morphology evolution of the $^{0.1}$UGS was monitored in order to illustrate the growth mechanism of UGS crystal. Fig. 5 shows the TEM images of silver nanoseeds and morphologies of $^{0.1}$UGS crystal at different growth time (defined as t). The TEM image of the silver seeds reveals that these nanoseeds were quasi-spherical particles with smooth surface, and about 40 nm in diameter (Fig. 5a). After the reactants were mixed for 15 s, small branched structures appeared (Fig. 5b). The different contrast of the solid core and the branches may indicate they were not made from the same materials or not generated at the same time. At $t = 25$ s, structures with more branches or bumps on their surface were produced (Fig. 5c), and the particle size increased compared with that of the branched structures obtained at $t = 15$ s. As the reaction proceeded to $t = 45$ s, product with larger size formed (Fig. 5d). Some large gold primary crystals attached to the product surface could also be observed, which indicates the gold source for the particle growth. In the following 30 s, large primary crystals gradually disappeared, and product with obvious urchin-like morphology was generated (Fig. 5e). However, most thorns of the UGS were decorated with

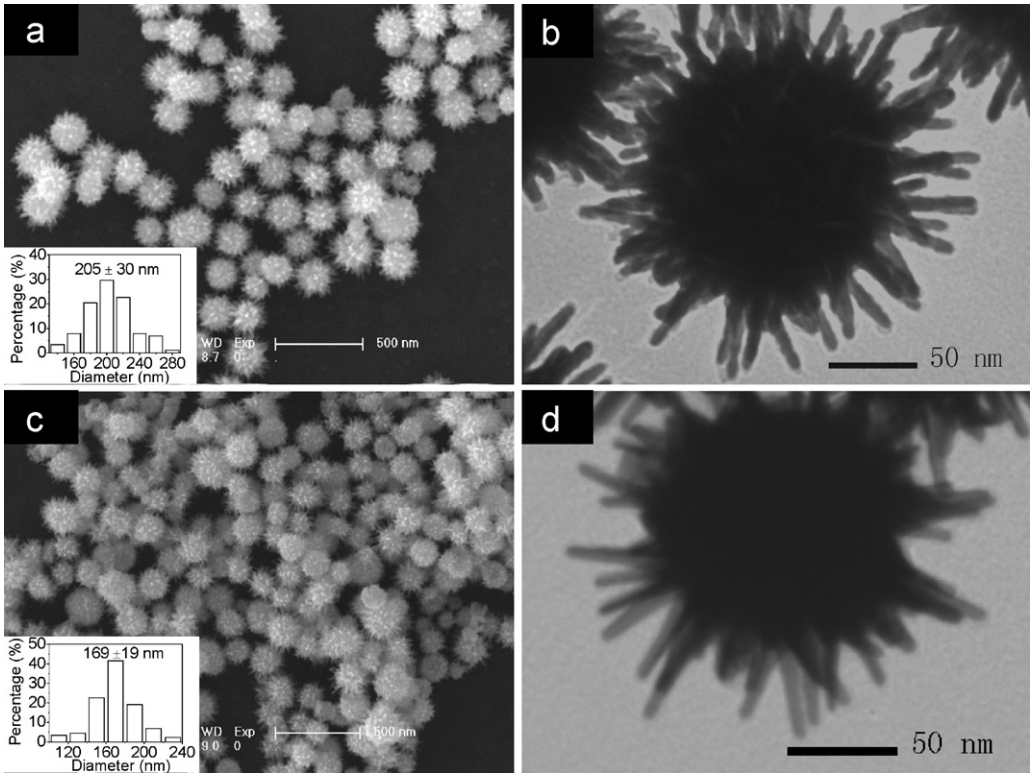

Fig. 4. SEM images (a and c) and enlarged TEM images (b and d) of UGS obtained at the presence of different amount of silver nanoseeds: (a and b) 0.2 mL seed, (c and d) 0.5 mL seed. The insets of Fig. 2a and c show the corresponding size distribution of these UGS.

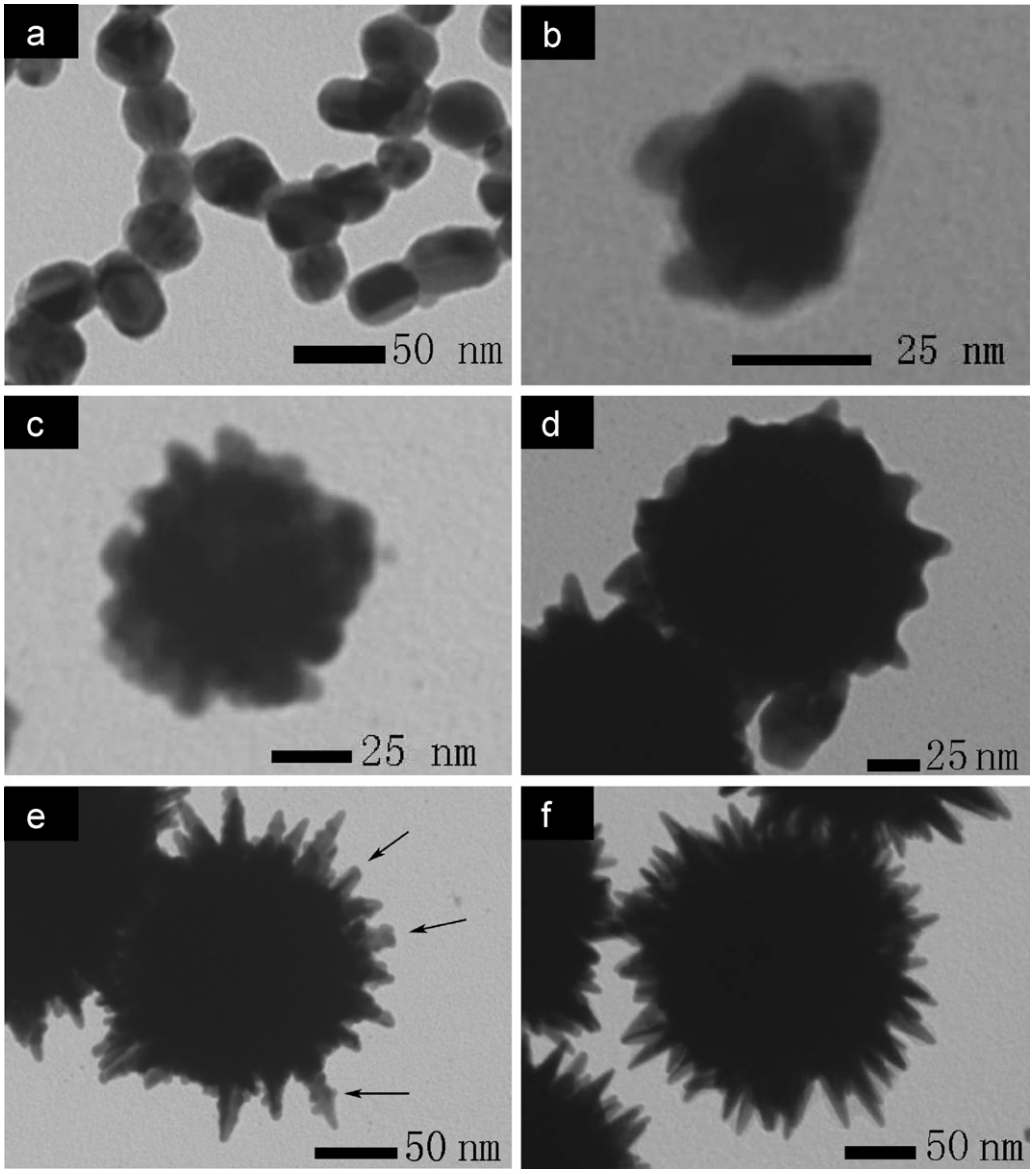

Fig. 5. TEM images of (a) silver nanoseeds and (b–f) UGS at different reaction time: (b) 15 s, (c) 25 s, (d) 45 s, (e) 75 s and (f) 180 s.

small primary crystals and some thorns were not intact (indicated by the arrow in Fig. 5e), which imply that the crystal growth was not completed. About 3 min later, well-shaped UGS with smooth nanothorns formed (Fig. 5f), and the decorated primary crystals disappeared, which may be due to the Ostwald ripening [34]. Further increasing the reaction time up to 12 h, no obvious change of morphology could be observed.

Based on the above results, a preliminary crystal growth mechanism was proposed. First, gold nuclei were generated through Dopa reduction and they fast grew into primary gold crystals. These primary crystals are not stable due to their high surface energy. So in the second step, these primary crystals will attach to the silver seeds to decrease their surface energy [35], and consequently, branched products were obtained. As the reaction proceeded, more gold primary crystals were generated and they continuously attached to the surface of the branched structures. Finally, the gold atoms of the attached primary crystals rearranged through the crystal ripening, which provided the gold source for the growth of branched structures into well-shaped UGS with more thorns. However the exact growth mechanism of UGS is not very clear at present time and further study is needed.

3.4. Electrochemical characterization of UGS

The urchin-like morphology and the relatively small diameter indicate these UGS may have larger active surface area than other hierarchical structures, such as flower-like gold submicrostructures (FGS) obtained here. To verify this hypothesis, the gold submicrostructures obtained at different reaction conditions in Section 3.2 were used to modify GCEs and cyclic voltammetric (CV) behaviors of these modified electrodes in 0.5 M H_2SO_4 were investigated. Fig. 6 shows the CVs of the bare gold electrode (3 mm in diameter) and electrodes modified by different gold submicrostructures including FGS, $^{0.1}$UGS, $^{0.2}$UGS, $^{0.5}$UGS obtained in Section 3.2 in 0.5 M H_2SO_4. As can be seen, these modified electrodes display much higher peak currents associated with oxide formation/reduction events than that of bare gold electrode (inset of Fig. 6). All the electrodes modified with UGS (UGS/GCE) exhibit larger current response than that of FGS (curve a of Fig. 6). This is mainly due to their relatively small size and urchin-like morphology, which endow them with more active surface area (Fig. 1c and d). For UGS obtained in the presence of different amount of silver nanoseeds, the peak current increases as the amount of the

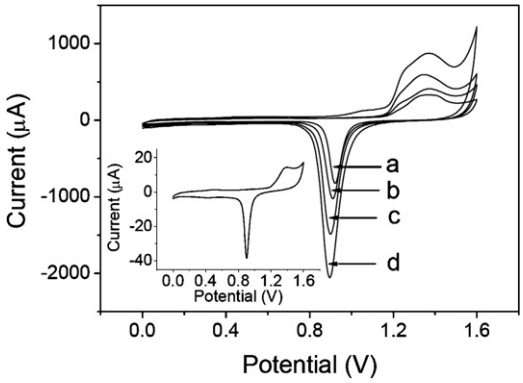

Fig. 6. The cyclic voltammograms of electrodes modified by different gold submicrostructures in 0.5 M H_2SO_4: (a) FGS/GCE, (b) $^{0.1}$UGS/GCE, (c) $^{0.2}$UGS/GCE and (d) $^{0.5}$UGS/GCE. The inset shows the response of bare gold electrode in the same solution.

added nanoseeds increases (curve b–d of Fig. 6), which could be ascribed to the small particle diameter. In brief, among all the electrodes modified with various gold submicrostructures obtained in this study, the $^{0.5}$UGS modified electrode ($^{0.5}$UGS/GCE) displays the highest peak current (curve d of Fig. 6). Therefore, it is expected that the $^{0.5}$UGS may have good performance in electrocatalysis, such as electrocatalytic oxidation of glucose.

3.5. Application of UGS in nonenzymatic glucose sensor

It is reported that gold nanostructures are good catalysts for oxidation of glucose and many nonenzymatic glucose sensors have been fabricated based on this catalysis [36,27]. The $^{0.5}$UGS obtained here with large surface to volume ratio inspired us to investigate their electrocatalytic activity towards the glucose oxidation.

The CVs of bare gold electrode, FGS/GCE and $^{0.5}$UGS/GCE in PBS solution (pH = 7.4) containing 50 mM glucose at 50 mV/s are exhibited in Fig. 7. As can be seen, these electrodes exhibit similar electrochemical behaviors. There is no obvious current response in the absence of glucose for these electrodes (dashed curve of Fig. 7). After glucose was added, the current increased and several peaks were observed (solid curve of Fig. 7). The CV process of glucose oxidation on $^{0.5}$UGS/GCE has been illustrated in Scheme 1. The first current peak in the CV at about 0.06 V could be ascribed to the electrosorption of glucose to form adsorbed intermediate, releasing one proton per glucose molecule (Scheme 1a and b) [36]. As the intermediates accumulate on the electrode surface, the active sites of the UGS electrode are occupied, inhibiting the direct oxidation of glucose. At more positive values, OH_{ads} are formed at the UGS surface, catalyzing the oxidation of the poisoning intermediates. As a result, free Au active sites are available for the direct oxidation of glucose, leading to the current peak at 0.32 V (Scheme 1b and c). As potential further moves positively, gold oxide is formed, which competes for surface adsorption sites with glucose, leading to the decrease of current response (Scheme 1c and d). In the negative direction scan, gold oxide is reduced and enough surface active sites are exposed for the direct oxidation of glucose, resulting in a sharp current peak at about 0.34 V (Scheme 1d and e). As the potential moving negatively, the electrosorption of glucose at the UGS starts again and intermediate accumulats on the electrode surface, resulting in the small increase in current from 0.2 to −0.1 V (Scheme 1f and g). Compared with that of bare gold electrode (solid curve in Fig. 7c) and FGS/GCE (solid curve in Fig. 7b), the $^{0.5}$UGS/GCE exhibited lower oxidation potential and much larger oxidation current, which clearly demonstrate the better electrocatalytic activity of the $^{0.5}$UGS towards the glucose oxidation.

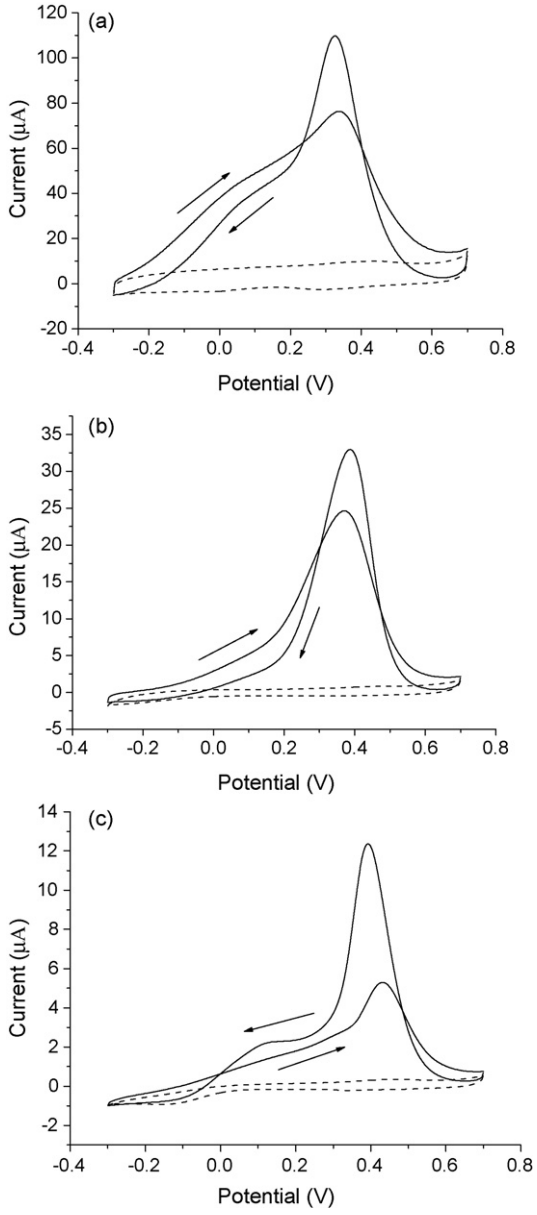

Fig. 7. The cyclic voltammogram of various electrodes in PBS (pH = 7.4) in the absence (dashed line) and in the presence of 50 mM glucose (solid line): (a) $^{0.5}$UGS/GCE, (b) FGS/GCE and (c) bare gold electrode.

The good catalytic activity of $^{0.5}$UGS inspired us to fabricate a nonenzymatic glucose sensor. Fig. 8 shows the typical amperometric responses of the $^{0.5}$UGS/GCE upon the successive injection of glucose into the PBS solution (pH = 7.4) at 0.32 V. Upon each addition of glucose, the $^{0.5}$UGS based sensor could reach the maximum steady current within 3 s, indicating a rapid amperometric response. This may be ascribed to the large surface to volume ratio of the $^{0.5}$UGS and its 3-D open structure, which could provide a good electron-conducting tunnel and allow the electron transfer to happen easily [37]. The linear range of this sensor is from 0.1 to 31.3 mM (inset of Fig. 8) with a sensitivity of 30.7 μA mM^{-1} cm^{-2}, and the detection limit is 4 μM (S/N = 3). This result is much better than previous reported glucose sensor based on porous gold materials [27], and the upper limit of the linear range is far beyond the physiological lever of glucose (3–8 mM). Compared with the amperometric response of FGS based sensor (the bottom curve of Fig. 8), the $^{0.5}$UGS based sensor displayed much higher sensitivity and wider linear range, which further confirms the advantages

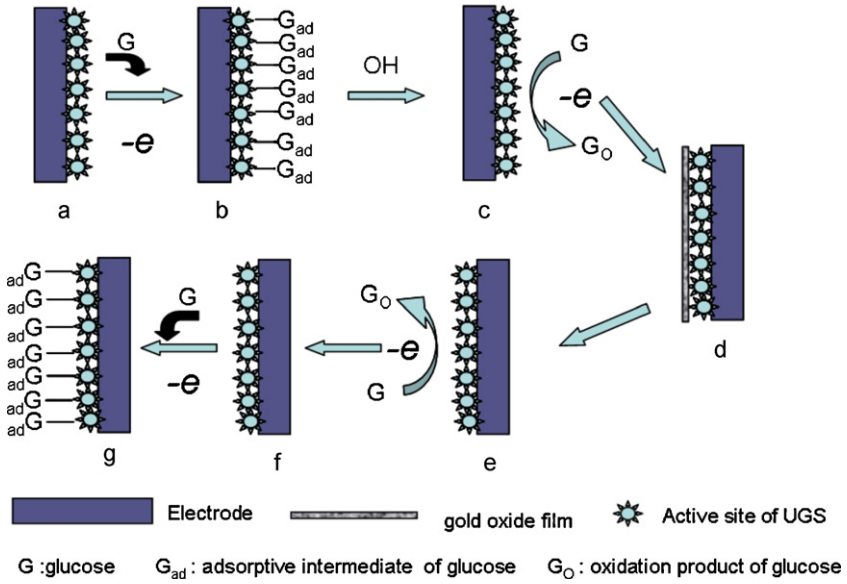

Scheme 1. Schematic illustration of the glucose oxidation on $^{0.5}$UGS/GCE.

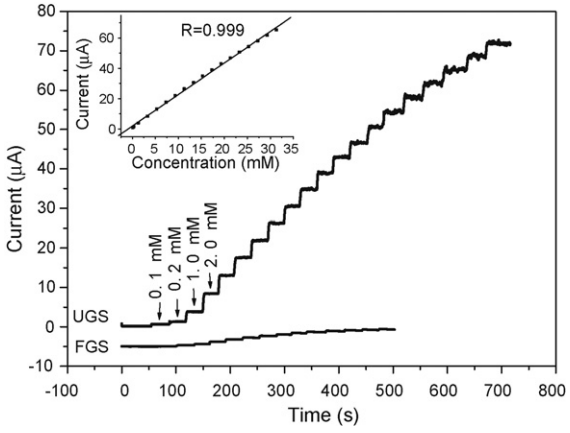

Fig. 8. The response of the $^{0.5}$UGS and FGS based sensors for the successive injection of glucose in PBS (pH = 7.4). Applied potential: 0.32 V vs. Ag/AgCl. The inset shows the calibration line of the response current vs. the glucose concentration of the $^{0.5}$UGS based sensor.

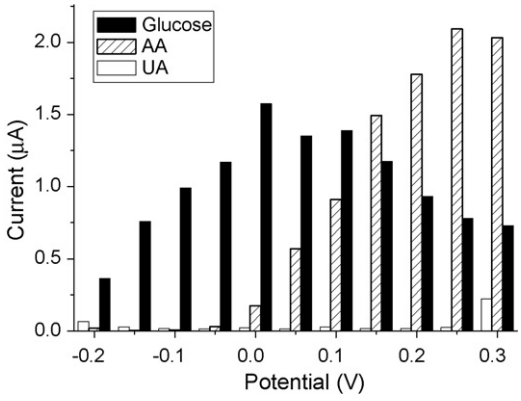

Fig. 9. The influence of different detection potentials on the selective detection of 3.0 mM glucose in the presence of 0.02 mM UA (uric acid) and 0.1 mM AA (ascorbic acid).

of the morphology and size control studied here. The response of $^{0.5}$UGS/GCE to the glucose oxidation was re-examined after it was stored at 4 °C for 40 days. It is observed that the catalytic potential was almost unchanged and the catalytic current only had a slight decrease (less than 15%, data not shown), indicating that the present sensor has a good stability for a long-term.

It is well known ascorbic acid and uric acid in the biological samples could be easily oxidized at positive potential and often interfere the detection of glucose. So an optimum detection potential should be selected for the detection of glucose without interference. Fig. 9 shows the response of $^{0.5}$UGS/GCE to UA, AA and glucose on the physiological level (UA 0.02 mM, AA 0.1 mM and glucose 3 mM) at different detection potentials. It is observed the interference of AA is serious at 0.32 V. However, this interference decreased dramatically when the detection potential shifts to

Table 1
Comparison of analytical performance of some glucose sensors.

Materials	Response time (s)	Linear range (mM)	Sensitivity ($\mu A\,mM^{-1}\,cm^{-2}$)	Refs.
Porous gold	2	2–10	11.8	[27]
Mesoporous Pt	>10	0–10	9.6	[38]
Pt nanotubules	≈10	2–14	0.1	[39]
Nanoporous Pt	≈15	1–10	1.65	[40]
[a]OMCs–GOD	9	0.5–15	0.75	[41]
[b]Gox–xGnP	5	0–6	14.17	[42]
[c]PS–PANI–Au–GOD	10	0.04–2.04	–	[43]
UGSs	3	0.2–13.2	16.8	This work

[a] OMCs–GOD–Nafion: ordered mesoporous carbon–glucose oxidase–Nafion composite film.
[b] Gox–xGnP: glucose oxidase loaded on exfoliated graphite.
[c] PS–PANI–Au–GOD: polystyrene–polyaniline–Au–glucose oxidase nanocomposite.

negative values. At potential of −0.05 V, the interference from UA to AA could be negligible and response of glucose still had relatively large current value. It is reported the oxidation of glucose on gold electrode initiated at about −0.2V(vs. SCE) [44,45], so it is believed the glucose could also be oxidized at −0.05 V, although the oxidation extent is small compared with that at 0.32 V. At this optimum potential, the detection linear range of the UGS based glucose sensor is 0.2–13.2 mM, which is also beyond the physiological level. The sensitivity is 16.8 $\mu A\,mM^{-1}\,cm^{-2}$ and the detection limit is 10 μM (S/N = 3). Table 1 compares the performance of this sensor with certain enzyme-based biosensors and inorganic materials based nonenzymatic sensor. It is clear the UGS based sensor displays a faster response, wider linear range and higher sensitivity, which indicate its potential application in nonenzymatic glucose sensing.

4. Conclusions

In summary, we developed a seed-mediated approach to prepare UGS, which could be used for nonenzymatic detection of glucose. The method presented in this work is quite facile. The morphologies and size of final products could be controlled by adding different amount of nanoseeds into the reactant solution. More importantly, the UGS with the relative small size and urchin-like morphology display higher surface to volume ratio than flower-like gold submicrostructures. As application, the UGS reveals a good catalytic activity for the glucose oxidation, and a nonenzymatic glucose sensor with fast response, well stability and good selectivity has been successfully fabricated based on the UGS material.

Acknowledgments

Financial support by the National Natural Science Foundation of China (20775077), the National Basic Research Program of China (973 Program, No. 2010CB933600) and the Chinese Academy of Sciences (KJCX2-YW-H11) is gratefully acknowledged.

References

[1] A.E. Espinal, L.C. Zhang, C.H. Chen, A. Morey, Y.F. Nie, L. Espinal, B.O. Wells, R. Joesten, M. Aindow, S.L. Suib, Nat. Mater. 9 (2010) 54–59.
[2] I.H. Hong, Y.C. Liao, S.C. Yen, Adv. Funct. Mater. 19 (2009) 3389–3395.
[3] S.M. Douglas, H. Dietz, T. Liedl, B. Hogberg, F. Graf, W.M. Shih, Nature 459 (2009) 414–418.
[4] Y. He, T. Ye, M. Su, C. Zhang, A.E. Ribbe, W. Jiang, C.D. Mao, Nature 452 (2008) 198–241.
[5] H. Kang, F.A. Detcheverry, A.N. Mangham, M.P. Stoykovich, K.C. Daoulas, R.J. Hamers, M. Muller, J.J. de Pablo, P.F. Nealey, Phys. Rev. Lett. 100 (2008) 148303.
[6] C.L. Nehl, J.H. Hafner, J. Mater. Chem. 18 (2008) 2415–2419.
[7] B.K. Jena, B.K. Mishra, S. Bohidar, J. Phys. Chem. C 113 (2009) 14753–14758.
[8] B.K. Jena, C.R. Raj, Langmuir 23 (2007) 4064–4070.
[9] J. Xie, Q. Zhang, J.Y. Lee, D.I.C. Wang, ACS Nano 12 (2008) 2473–2480.
[10] L. Lu, K. Ai, Y. Ozaki, Langmuir 24 (2008) 1058–1063.
[11] S. Cherevko, C.H. Chung, Sens. Actuators B 142 (2009) 216–223.
[12] S. Guo, L. Wang, E. Wang, Chem. Commun. 30 (2007) 3163–3165.
[13] L. Lu, I. Randjelovic, R. Capek, N. Gaponik, J. Yang, H. Zhang, A. Eychmuller, Chem. Mater. 17 (2005) 5731–5736.
[14] H. Wang, N.J. Halas, Adv. Mater. 20 (2008) 820–825.
[15] J.H. Kim, T. Kang, S.M. Yoo, S.Y. Lee, B. Kim, Y.K. Choi, Nanotechnology 20 (2009) 235302.
[16] J.H. Kim, X.J. Huang, Y.K. Choi, J. Phys. Chem. C 112 (2008) 12747–12753.
[17] F.Q. Sun, J.C. Yu, Angew. Chem. Int. Ed. 46 (2007) 773–777.
[18] W.T. Wu, W. Pang, G. Xu, L. Shi, Q. Zhu, Y. Wang, F. Lu, Nanotechnology 16 (2005) 2048–2051.
[19] L. Lu, A. Kobayashi, K. Tawa, Y. Ozaki, Chem. Mater. 18 (2006) 4894–4901.
[20] B.S. Ljukic, C.E. Banks, C. Salter, A. Crossley, R.G. Compton, Analyst 131 (2006) 670–677.
[21] D. Shan, J. Zhang, H.G. Xue, S.N. Ding, S. Cosnier, Biosens. Bioelectron. 25 (2010) 1427–1433.
[22] M. Wang, W. Zhang, B. Fang, Chin. J. Anal. Chem. 38 (2010) 125–128.
[23] H. Wei, E. Wang, Anal. Chem. 80 (2008) 2250–2254.
[24] J. Li, Y.B. Wang, J.D. Qiu, D.C. Sun, X.H. Xia, Anal. Bioanal. Chem. 383 (2005) 918–922.
[25] J.D. Qiu, H.P. Peng, R.P. Liang, Electrochem. Commun. 9 (2007) 2734–2738.
[26] D. Rathod, C. Dickinson, D. Egan, E. Dempsey, Sens. Actuators B 143 (2010) 547–554.
[27] Y. Li, Y.Y. Song, C. Yang, X.H. Xia, Electrochem. Commun. 9 (2007) 981–988.
[28] P.C. Lee, D. Meisel, J. Phys. Chem. 86 (1982) 3391–3395.
[29] Y. Sun, Y. Xia, Science 298 (2002) 2176–2179.
[30] L. Wang, J. Bai, Y. Li, Y. Huang, Angew. Chem. Int. Ed. 47 (2008) 2439–2442.
[31] S. Guo, D. Wen, S. Dong, E. Wang, Talanta 77 (2009) 1510–1517.
[32] G. Duan, W. Cai, Y. Luo, Z. Li, Y. Li, Appl. Phys. Lett. 89 (2006) 211905.
[33] A. Gole, C.J. Murphy, Chem. Mater. 16 (2004) 3633–3640.
[34] W.F. Ostwald, Phys. Chem. 22 (1897) 289–330.
[35] L. Charlis, S. Wolfgang, Adv. Funct. Mater. 15 (2005) 1197–1208.
[36] H. Zhang, J.J. Xu, H.Y. Chen, J. Phys. Chem. C 112 (2008) 13886–13892.
[37] H.C. Shin, M.L. Liu, Adv. Funct. Mater. 15 (2005) 582.
[38] S. Park, T.D. Chung, H.C. Kim, Anal. Chem. 75 (2003) 3046–3049.
[39] J.H. Yuan, K. Wang, X.H. Xia, Adv. Funct. Mater. 15 (2005) 803–809.
[40] S. Joo, S. Park, T.D. Chung, H.C. Kim, Anal. Sci. 23 (2007) 277–281.
[41] M. Zhou, L. Shang, B. Li, L. Huang, S. Dong, Biosens. Bioelectron. 24 (2008) 442.
[42] J. Lu, L.T. Drzal, R.M. Worden, I. Lee, Chem. Mater. 19 (2007) 6240.
[43] Y. Liu, X. Feng, J. Shen, J. Zhu, W. Hou, J. Phys. Chem. B 112 (2008) 9237–9242.
[44] M.W. Hsiao, R.R. Adzic, E.B. Yeager, J. Electrochem. Soc. 143 (1996) 759–767.
[45] W. Zhao, J.J. Xu, C.G. Shi, H.Y. Chen, Electrochem. Commun. 8 (2006) 773–778.